



RESEARCH LETTER

10.1002/2017GL074972

Key Points:

- Heat uptake over the Southern Ocean under global warming has pronounced influences on global atmospheric circulations
- The delayed warming over the Southern Ocean extends northward to the tropics, shifting the tropical precipitation northward
- Distinct zonal variations in tropical SST and precipitation responses develop, accompanying the interhemispheric asymmetry

Supporting Information:

- Supporting Information S1

Correspondence to:

Y.-T. Hwang,
yhwang@ntu.edu.tw

Citation:

Hwang, Y.-T., S.-P. Xie, C. Deser, and S. M. Kang (2017), Connecting tropical climate change with Southern Ocean heat uptake, *Geophys. Res. Lett.*, *44*, doi:10.1002/2017GL074972.

Received 19 JUL 2017

Accepted 11 AUG 2017

Accepted article online 16 AUG 2017

Connecting tropical climate change with Southern Ocean heat uptake

Yen-Ting Hwang¹ , Shang-Ping Xie² , Clara Deser³ , and Sarah M. Kang⁴ 

¹Department of Atmospheric Sciences, National Taiwan University, Taipei, Taiwan, ²Scripps Institution of Oceanography, University of California San Diego, La Jolla, California, USA, ³Climate and Global Dynamics, National Center for Atmospheric Research, Boulder, Colorado, USA, ⁴School of Urban and Environmental Engineering, Ulsan National Institute of Science and Technology, Ulsan, South Korea

Abstract Under increasing greenhouse gas forcing, climate models project tropical warming that is greater in the Northern than the Southern Hemisphere, accompanied by a reduction in the northeast trade winds and a strengthening of the southeast trades. While the ocean-atmosphere coupling indicates a positive feedback, what triggers the coupled asymmetry and favors greater warming in the northern tropics remains unclear. Far away from the tropics, the Southern Ocean (SO) has been identified as the major region of ocean heat uptake. Beyond its local effect on the magnitude of sea surface warming, we show by idealized modeling experiments in a coupled slab ocean configuration that enhanced SO heat uptake has a profound global impact. This SO-to-tropics connection is consistent with southward atmospheric energy transport across the equator. Enhanced SO heat uptake results in a zonally asymmetric La-Nina-like pattern of sea surface temperature change that not only affects tropical precipitation but also has influences on the Asian and North American monsoons.

1. Introduction

Robust patterns of sea surface temperature (SST) and rainfall response to global warming have been identified in recent studies. For example, almost all models participating in the Coupled Model Intercomparison Project Phase 3 and Phase 5 (CMIP3 and CMIP5) show a larger increase in SST and rainfall over the northern than southern tropics by the end of the 21st century [Xie *et al.*, 2010; Friedman *et al.*, 2013; Liu *et al.*, 2005]. Further, the delayed warming and drying trend in the southern tropics exhibit zonal asymmetries, being most pronounced over the southeastern portion of the ocean basins. These subtropical drying regions also extend to the western coasts of continents at the edge of the Hadley Cell, over South America, southern Africa, and Australia (see Figure SPM.7 in *Intergovernmental Panel on Climate Change* [2014]).

The hemispheric asymmetry of tropical SST and rainfall changes is associated with an intensification of the southeast trades and a slight weakening of the northeast trades. The strengthened southeasterly trade winds enhance sea surface evaporation, and further cool the SST. This wind-evaporation-SST (WES) feedback indicates the importance of ocean-atmosphere interaction but does not explain why the Northern Hemisphere (NH) warms faster than the Southern Hemisphere (SH) [Xie *et al.*, 2010].

Another well-known SST response pattern is the muted warming over the SO where upwelling and deep vertical mixing occur [Manabe *et al.*, 1991; Marshall *et al.*, 2014]. In CMIP5 models, more than half of the excess heat due to increased radiative forcing is stored in the SO over the past century [Frölicher *et al.*, 2015; Kuhlbrodt and Gregory, 2012]. Indeed recent observations suggest the SO accounts for most of the heat storage (67 to 98%) over the past decade (2006 to 2013) [Roemmich *et al.*, 2015]. SO heat uptake has been recognized as an important factor affecting many aspects of the climate response to increased greenhouse gas (GHG), including westerly winds over the SO, Antarctic sea ice, and climate sensitivity [Manabe *et al.*, 1991; Raper *et al.* 2002; Armour *et al.*, 2013]. In addition to the effects in the SH extratropics, some recent studies have investigated its nonlocal influences on patterns of climate feedbacks [Rose *et al.*, 2014; Rugenstein *et al.*, 2016; Rose and Rencurrel, 2016]. Furthermore, Cabre *et al.* [2017] have identified a global scale teleconnection driven by multidecadal SO convection.

Here we design two sets of idealized coupled model experiments in a slab ocean setting, described in section 2, to explore the influence of Southern Ocean heat uptake on global atmospheric circulation, with a focus on its remote influence on tropical climate. In addition to the zonal-mean changes in Hadley

Circulation that can be understood within the framework of energetic constraints [Kang *et al.*, 2008; Hwang *et al.*, 2013; Schneider *et al.*, 2014] (section 3.1), we investigate the zonally asymmetric response shaped by the climatological wind pattern and cloud properties (sections 3.2–3.3). We compare our coupled slab ocean model results with fully coupled models that include dynamical ocean processes in section 4 and summarize our findings in section 5.

2. Experimental Design

We perform two sets of idealized experiments with the Community Atmospheric Model version 5 (CAM5) coupled to a motionless slab ocean. The model features active sea ice and realistic land-sea distributions and topography. We use the default q -flux that aims to reproduce the climatological SST distribution from the fully coupled Community Earth System Model version 1 (CESM1) of which CAM5 is the atmospheric component [see He *et al.*, 2017]. In both experiments, we prescribe an abrupt quadrupling of CO₂ and perform a 20 year simulation. In the control experiment (hereafter termed *control*), we use a constant mixed-layer depth (MLD) of 50 m. In the perturbation experiment (hereafter termed *deepSO*), we set the MLD to 500 m over the region 40–80°S to mimic the effects of enhanced SO heat uptake; elsewhere, the MLD remains at 50 m. The 500 m MLD value over the entire SO is not meant to be realistic [see de Boyer Montégut *et al.*, 2004] but is designed to mimic the key effects of the SOs climatological meridional overturning circulation (MOC) that make SH middle-to-high latitudes an optimal spot for heat uptake, e.g., the effects of upwelling of cold deep water and advection by equatorward Ekman flow which spreads the absorbed heat to the north of the upwelling branch of the MOC [Marshall *et al.*, 2014; Armour *et al.*, 2016]. The magnitude of the change in net surface energy flux over the SO in response to a quadrupling of CO₂ in the deepSO experiment is comparable to that in the CMIP5 models (e.g., models with a dynamical ocean; Figure S1). We evaluate the effects of enhanced SO heat uptake by comparing the responses to CO₂ quadrupling in the deepSO and control experiments. The evolution of zonal-mean SST after quadrupling CO₂ in deepSO and control experiments can be seen in Figure S2. During years 10–19, the control experiment approaches quasi-steady equilibrium with amplified zonal-mean warming at high latitudes in both hemispheres. In contrast, there is significantly less warming in middle-to-high latitudes in deepSO by this time.

3. Results

3.1. Zonal Mean Responses

We focus on the difference between the average of years 10–19 after quadrupling CO₂ and the 20 year average climatology under preindustrial CO₂ in the two experiments. The zonal mean responses of SST, meridional mass stream function, and precipitation in the two experiments and their differences are plotted in Figure 1. The polar amplified warming in the control run is slightly larger in the NH than the SH due presumably to the different land-sea distributions; there is also greater warming in the northern tropics compared to the southern tropics (Figure 1a). The meridional asymmetry in the control experiment is weak compared to that in the deepSO experiment (compare Figure 1a and Figure 1b). As expected, a deep MLD in the SO mutes the surface warming response at high southern latitudes [Manabe *et al.*, 1991; Marshall *et al.*, 2014; Armour *et al.*, 2016]. Remarkably, however, the muted surface warming extends all the way into the tropics, creating a strong asymmetry across the equator. The enhanced heat uptake over the SO reduces the overall warming; the tropical-mean (20°N–20°S) SST increase is reduced from 5.4 K in the control to 3 K in deepSO. The enhanced heat uptake also increases the interhemispheric tropical SST asymmetry (obtained by subtracting the average over 0–20°S from the average over 0–20°N) from 0.54 K in control to 1.36 K in deepSO.

In addition to interhemispheric tropical SST asymmetry, the responses of the atmospheric overturning circulation also exhibit distinct characteristics in the two experiments (Figures 1d and 1e). Gross moist stability, the ratio between energy and mass fluxes, changes by about 30% at the equator in our experiments. The change is small enough to allow us to interpret the relationships between energy, mass, and moisture transport within the energetic framework proposed in previous studies [Chiang and Bitz, 2005; Kang *et al.*, 2008; Hwang *et al.*, 2013; Schneider *et al.*, 2014; Chiang and Friedman, 2012]. In response to SO heat uptake, an anomalous thermally direct meridional atmospheric overturning circulation develops to adjust to the hemispheric asymmetry: Anomalous northerly flow aloft transports air with high gravitational potential energy to the southern tropics (red arrow in Figure 1f), and the southerly return flow at low levels transports moisture to

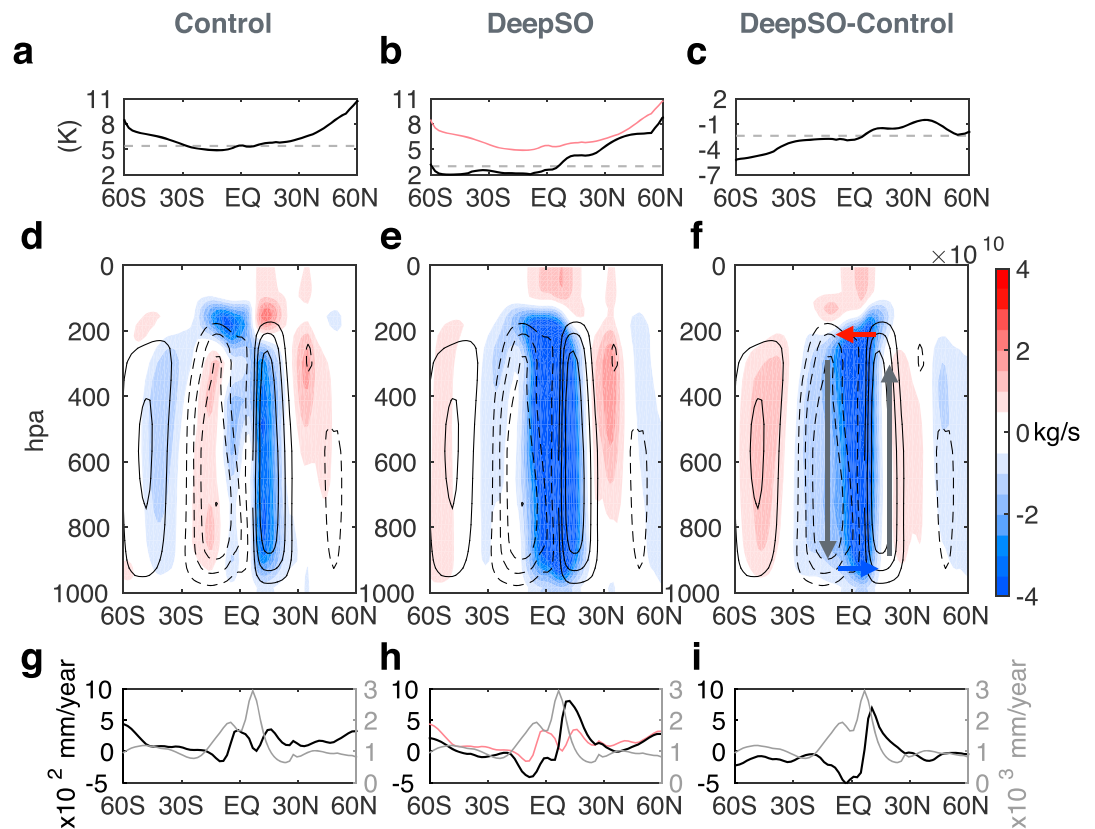


Figure 1. Zonal mean responses to an abrupt quadrupling of CO₂ in coupled slab-ocean experiments. (a–c) Responses of zonal mean SST (black solid line) and tropical mean (20°S–20°N) SST (dashed line) in control, deepSO, and deepSO minus control. (d–f) Responses of meridional mass stream function (shading) in control, deepSO, and deepSO minus control. Black contours show the climatological mass stream function (contour interval of 2.5×10^{10} kg/s). In Figure 1f, the red arrow refers to anomalous southward energy transport, the blue arrow refers to anomalous northward moisture transport, and the grey arrows indicate anomalous upward and downward motion. (g–i) Responses of zonal mean precipitation (mm/yr $\times 100$; black line) in control, deepSO and deepSO minus control. The thin grey lines show the climatological zonal mean precipitation. The responses from control are added in Figures 1b and 1h in light red line for easy comparison with deepSO.

the NH (blue arrow in Figure 1f). The anomalous meridional circulation is accompanied by changes in vertical motion (grey arrows in Figure 1f, upward north and downward south of the equator) that correspond to increased precipitation and drying, respectively (Figure 1i). The precipitation centroid, defined as the precipitation centroid between 20°S and 20°N, shifts northward by 2.3° of latitude, and the anomalous cross-equatorial atmospheric energy transport changes by 0.5 PW, in deepSO (see Figure 1h for precipitation changes; energy transport is not shown). This is in contrast to the more symmetric circulation changes with little anomalous cross-equatorial atmospheric energy transport (Figure 1d), along with a moistening trend at the equator and a drying trend on either side (Figure 1g) in control. The difference between deepSO and control shows a 2.1° northward shift of the precipitation centroid and a southward cross-equatorial atmospheric energy transport of 0.65 PW (see Figure 1i for precipitation changes; energy transport is not shown); the ratio between the precipitation shift and energy transport change is similar to that based on interannual variability in reanalysis data (1%/0.34 PW: Donohoe et al. [2014]).

3.2. Patterns of SST and Precipitation Response

Patterns of SST, surface wind, and precipitation response are plotted in Figure 2. The effects of enhanced SO heat uptake are comparable in magnitude to, but distinct in spatial pattern from, GHG-forced climate change as simulated by a slab ocean model of uniform MLD (compare Figures 2a with 2c and Figures 2d with 2f). While the MLD perturbation in deepSO is zonally uniform, the climate change response exhibits marked

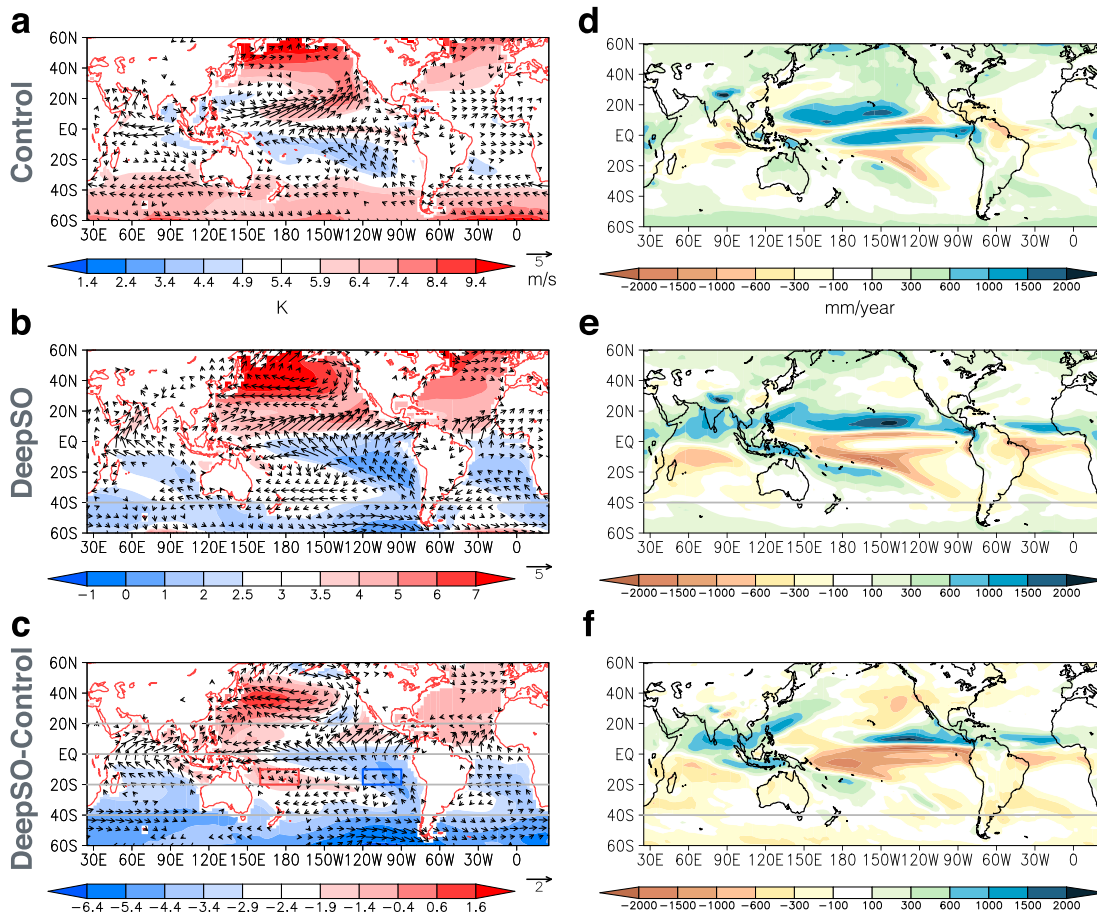


Figure 2. Spatial patterns of response to an abrupt quadrupling of CO₂ in coupled slab ocean experiments. Responses in near surface wind (vectors, Figures 2a–2c, m/s), SST (shading, Figures 2a–2c, K), and precipitation (shading, Figures 2e–2f, mm/yr) in (a and d) control, (b and e) deepSO, and (c and f) their difference. Note that the color bars in Figures 2a–2c are centered on the tropical mean value, with red (blue) denoting SST changes larger (smaller) than the tropical mean. An attribution analysis for the asymmetric warming in the blue box and the red box in Figure 2c is presented in section 3.3 and Figure 3.

zonal variations at low latitudes (Figures 2b and 2e), especially in the southern subtropics. The zonal variations are mainly due to the SO heat uptake effect, obtained by differencing the deepSO and control experiments (Figures 2c and 2f). The SO heat uptake alters the meridional temperature gradient, leading to intensified trade winds over the southeast ocean basins, expansion and strengthening of the subtropical highs, and drying in South America, southwest Australia, and south of Africa (Figures 2c and 2f).

In addition to delayed warming and enhanced drying in eastern oceanic basins in southern subtropics, the anomalous meridional circulation is accompanied by anomalous easterlies, increased zonal gradient, and a strengthened Walker Circulation in the deep tropics (Figure 2c). The enhanced east-west SST gradient shifts the convective region from the Pacific warm pool to the Maritime Continent, similar to that which occurs during La Niña events. The anomalous tropical SST pattern and associated change in tropical convection may trigger a Rossby wave train with northward energy propagation and drive the circulation changes in the North Pacific [Ting and Sardeshmukh, 1993; Trenberth et al., 1998]. In particular, the Aleutian low pressure system weakens, bringing warm, moist air to the western North Pacific and Asia, and cold, dry air to the eastern North Pacific and North America.

3.3. Attribution of the Zonally Asymmetric SST Response in the Tropical South Pacific Based On Surface Energy Budget Analysis

In section 3.2, we reported an enhanced east-west SST gradient associated with the increased interhemispheric SST gradient in control and deepSO. Figure 3a demonstrates this linear relationship between north-south and east-west asymmetries. The linear relationship exists in all ocean basins, but it is most

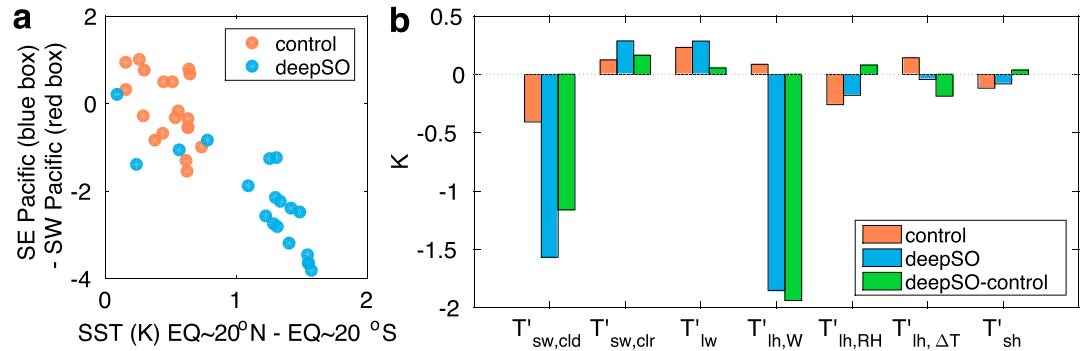


Figure 3. The east-west SST asymmetry. (a) Anomalous zonal mean tropical SST asymmetry (anomalous SST in EQ ~ 20°N minus EQ ~ 20°S) versus anomalous eastwest SST asymmetry in southern tropical Pacific basin (anomalous SST in the blue box (120°W ~ 90°W, 10 ~ 20°S) minus the red box (160°E ~ 170°W, 10 ~ 20°S) in Figure 2c). Blue dots are from deepSO experiment and red dots are from control experiment. Each dot is the annual average of 1 year; and there are 19 dots for each experiment (year 1 ~ 19 after quadrupling CO₂). (b) The attribution of the east-west SST asymmetry. See equations (S1)–(S7) for details of the calculations and the definitions of each term. From left to right, the seven groups of bars refer to the contribution to east-west SST asymmetry by (1) changes in shortwave cloud radiative forcing ($T'_{sw,cl,d}$), (2) changes in shortwave radiation in clear sky ($T'_{sw,clr}$), (3) changes in longwave radiation (T'_{lw}), (4)–(6) changes in evaporation due to changes in wind ($T'_{lh,W}$), relative humidity ($T'_{lh,RH}$), stability ($T'_{lh,\Delta T}$), and (7) changes in sensible heat flux (T'_{sh}), respectively. The changes are calculated as in Figures 1 and 2 (the differences between the average of years 10–19 after quadrupling CO₂ concentration and climatology). Blue bars are from deepSO, red bars are from control, and green bars are the differences of the two experiments (deepSO-control). The term with negative green bars contribute positively to the differences in east-west asymmetry in the two experiments.

significant in the southern tropical Pacific. In order to understand the cause of this east-west asymmetry, we perform an energy budget analysis of the mixed layer ocean, which can be written as

$$\rho C_p H \frac{\partial T}{\partial t} = Q'_{sw} + Q'_{lw} + Q'_{lh} + Q'_{sh} + O' \quad (1)$$

[Xie *et al.*, 2010; Deser *et al.*, 2010]. The term on the left-hand side is the storage term (or the tendency term), which is very close to zero in the quasi-equilibrium tropics. ρ is density, C_p is the specific heat of seawater, H is mixed layer depth, and $\frac{\partial T}{\partial t}$ is temperature tendency. Following Xie *et al.* [2010], Jia and Wu [2013], and Zhang and Li [2014], we can rewrite equation (1) as a diagnostic equation for changes in SST (equation (2) below). Please see the supporting information for the detailed derivation. In brief, based on the linearized bulk formula for evaporation, the latent heat flux can be decomposed to changes related to (1) variations in wind speed, (2) variations in relative humidity, (3) variations in air-sea temperature difference, and (4) a term proportional to climatological evaporation and SST anomaly (i.e., the change in evaporation in the absence of changes in wind speed, relative humidity, and air-sea temperature difference). We can then organize the equation, making it a diagnostic equation for SST anomaly:

$$T' = T'_{sw,cl,d} + T'_{sw,clr} + T'_{lw} + T'_{lh,W} + T'_{lh,RH} + T'_{lh,\Delta T} + T'_{sh} \quad (2)$$

T' is changes in SST. The seven terms on the right-hand side refer to changes in SST due to different factors, they are changes in shortwave cloud radiative forcing, changes in shortwave radiation in clear sky, changes in longwave radiation, changes in latent heat flux due to variations in wind, relative humidity, or stability, and changes in sensible heat flux, respectively.

Figure 3b examines each term in equation (2) in the southeastern Pacific minus the same term in the southwestern Pacific (the blue box minus the red box in Figure 2c). Negative values contribute to increasing east-west SST gradient (larger warming in the west compared to the east).

The changes in latent heat flux related with wind changes ($T'_{lh,W}$ term in Figure 3b) explain some of the enhanced east-west asymmetry over the southern tropical Pacific in deepSO relative to control. The intensification of the southeast trades discussed previously is most significant in eastern oceanic basins. The prevailing southeast trade winds are favorable for this WES feedback, whereas the mean winds in the western basins

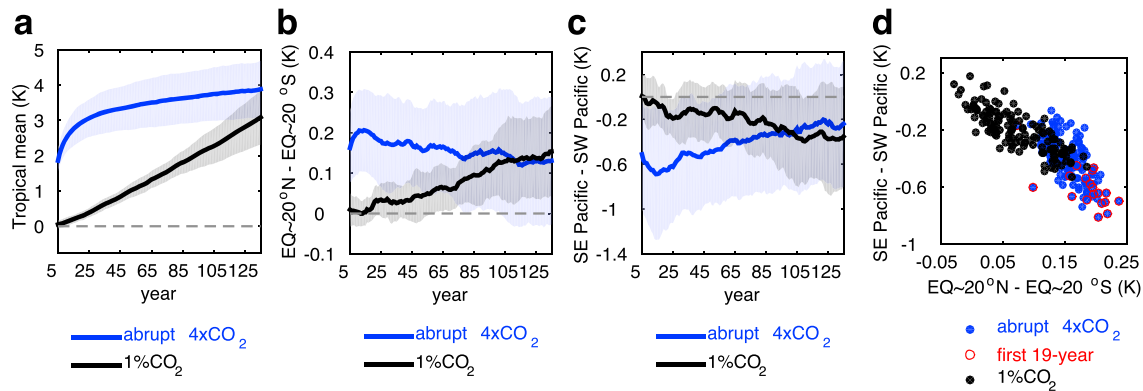


Figure 4. The N-S and E-W asymmetries in CMIP5 fully coupled models. Time series of (a) anomalous tropical mean SST, (b) anomalous zonal mean tropical SST asymmetry (anomalous SST in EQ ~ 20°N minus EQ ~ 20°S), and (c) anomalous east-west SST asymmetry in southern tropical Pacific basin (the blue box (120°W ~ 90°W, 10 ~ 20°S) minus the red box (160°E ~ 170°W, 10 ~ 20°S) labeled in Figure 2c) in CMIP5 fully coupled models in abrupt 4 × CO₂ and 1%CO₂ experiments. Black lines are ensemble means of 1%CO₂ experiment, and blue lines are ensemble mean of abrupt 4 × CO₂ experiment. Shading represents one standard deviation of model spread. A 10 year running mean is applied to the time series. (d) Anomalous zonal mean tropical SST asymmetry versus anomalous east-west SST asymmetry in southern tropical Pacific basin. Black dots are from 1%CO₂ experiment and blue dots are from abrupt 4 × CO₂ experiment. The dots of the first 19 years of abrupt 4 × CO₂ experiment are labeled with red open circles. Each dot is annual average of 1 year of ensemble model mean.

are less organized, with a small northerly component due to the subtropical high. Thus, the climatological circulation links the meridional asymmetry with the zonal asymmetry. Note that the changes in wind speed are more significant in the monthly mean wind field compared with the annual mean wind field plotted in Figure 2c. The WES feedback has been recognized as a key factor leading to the delayed warming over southeast ocean basins [Xie *et al.*, 2010]. There are northwest-southeast oriented cooling patches in the southern tropics in all three ocean basins.

In addition to WES feedback, shortwave cloud radiative forcing ($T'_{sw, cld}$ term in Figure 3b) also contributes significantly to the enhanced east-west asymmetry over the southern tropical Pacific in deepSO relative to control. Low stratus clouds over the cold eastern basins amplify SST perturbations, while high convective clouds over warm western basins damp them. With reduced warming, stratus clouds increase in deepSO (relative to control), leading to decreasing shortwave cloud radiative forcing in eastern basins. There is also less warming in the western ocean basins in deepSO (relative to control) where the cloud radiative effect is opposite: convective clouds decrease, leading to increased shortwave radiation at the surface.

The link between meridional and zonal SST gradients was previously recognized by Chiang *et al.* [2008] and Fedorov *et al.* [2015]. While these studies concern equatorial upwelling and the equatorial zonal SST gradient, the mechanisms of the east-west asymmetries we report here are related to atmospheric processes and thermodynamic ocean-atmosphere interactions in the subtropics. Controlled by climatological wind field and cloud properties, the zonal gradient associated with the hemispheric asymmetry is most significant in southern subtropical ocean basins in our experiments.

4. Comparison With CMIP5 Fully Coupled Models

The simplicity of the experimental design allows us to demonstrate causal relationships and highlight the global response to enhanced ocean heat uptake through atmospheric teleconnections and thermodynamic air-sea coupling. Since the only difference between deepSO and control is the MLD over 40°S–80°S, all of the response patterns in Figures 2c and 2f can be attributed to enhanced SO heat uptake. However, caution should be taken when quantifying the uncertainties of these responses.

To evaluate the role of dynamical ocean processes, Figure 4 shows the time evolution of relevant quantities in the CMIP5 models. In abrupt 4xCO₂ experiments, the tropical mean temperature increases rapidly during the first 20 years (Figure 4a). This rapid warming is not spatially uniform, with northern tropics warming faster than the southern tropics (Figure 4b) and southeastern Pacific warming less than southwestern Pacific (Figure 4c). The linear relationship between hemispheric asymmetry and zonal SST gradient in southern subtropical Pacific also holds for CMIP5 models (Figure 4d). The ratio between the meridional and zonal

asymmetry are remarkably similar in the idealized slab ocean and the CMIP5 dynamical ocean models, with the linear regression slopes being 1 K tropical hemispheric asymmetry corresponding to 2.6 K zonal SST gradient in southern subtropical Pacific in both Figures 3b and 4d.

Although the mean tropical SST increase is similar to our idealized deepSO experiment (3 K), the hemispheric asymmetry in warming is significantly reduced in the fully coupled models, which is likely due to the compensation from the shallow oceanic overturning cells connecting the subtropics and tropics [Held, 2001; Schneider *et al.*, 2014]. As the easterly trades strengthen in the southern tropics and weaken in the northern tropics, the anomalous winds induce an anomalously southward near-surface Ekman flow. The anomalous southward Ekman flow in both hemispheres transports warm water across the equator, decreases the hemispheric asymmetry in warming, and reduces the cross-equatorial atmospheric energy transport [Green and Marshall, 2017].

Another complication arises due to the slowdown of the Atlantic Meridional Overturning Circulation (AMOC) in response to CO₂ increase [Held *et al.* 2010; Cheng *et al.*, 2013]. As the northward transport of AMOC decrease, warming in the NH and N-S asymmetry also reduces. About 15 years after CO₂ quadrupling, some models show a gradual reduction in the N-S and E-W asymmetries (blue lines in Figures 4b and 4c) while the tropical mean SST continues to increase (blue line in Figure 4a). The reversal of hemispheric asymmetry is not apparent in the more realistic 1%CO₂ experiments; the N-S and E-W asymmetries both increase with time, with N-S asymmetry becoming more positive and E-W asymmetry becoming more negative throughout throughout the 140 years of the experiments (black lines in Figures 4b and 4c).

5. Summary

Our coupled slab ocean model experiments reveal that enhanced SO heat uptake has global impacts, especially with regard to the hemispheric asymmetry in GHG-induced climate response. Specifically, enhanced heat uptake by the SO reduces the surface ocean warming over the entire SH and drives a cross-equatorial Hadley circulation that displaces the tropical rain belt north of the equator. In addition to the cross-equatorial asymmetry that is consistent with the zonal mean energetic theories [Kang *et al.*, 2008; Frierson and Hwang 2012; Schneider *et al.*, 2014], marked zonal variations develop in response to the MLD deepening in the SO. In southern subtropical oceans, we report a linear relationship between hemispheric asymmetry and zonal SST gradient, resulting from zonal variations in climatological wind and clouds. In the equatorial Pacific, a La Niña-like pattern of sea surface temperature change develops and causes a westward shift of deep convection, a drying trend in the southeast subtropical ocean, and a weakened Aleutian Low. These zonal asymmetries in the southern subtropics and North Pacific are similar to those resulting from aerosol forcing or North Atlantic freshening, albeit with opposite sign and less pronounced thermal changes in the NH extratropics [Hill *et al.*, 2015; Xie *et al.*, 2013; Zhang and Delworth, 2005]. Similar SST or precipitation patterns emerge associated with the CMIP5 intermodel spread in the strength of Atlantic Meridional Overturning circulation or shortwave cloud forcing over SO [Wang *et al.*, 2014, Figure 1; Hwang and Frierson, 2013, Figure S1]. Identifying SO heat uptake as an important cause for hemispheric asymmetry and zonally varying SST changes is a step toward understanding and predicting patterns of precipitation and atmospheric circulation changes under global warming.

The characteristics associated with enhanced SO heat uptake are significantly weaker in the CMIP5 models than in a slab mixed layer ocean. The wind-driven subtropical cells in the ocean act as negative feedbacks to the hemispheric asymmetry. The degree of compensation from ocean dynamics appears to vary significantly across models, however. Understanding how the dynamical ocean modulates the climate response to different forcings is currently an active research area [Deser *et al.*, 2015, Tomas *et al.* 2016, Kay *et al.*, 2016, Hawcroft *et al.*, 2016, Green and Marshall, 2017]. The idealized slab ocean experiments we present here can serve as a reference for future evaluation of ocean dynamical effects compensating the hemispheric asymmetries due to SO heat uptake.

References

- Armour, K. C., C. M. Bitz, and G. H. Roe (2013), Time-varying climate sensitivity from regional feedbacks, *J. Clim.*, 26, 4518–4534.
- Armour, K. C., J. Marshall, J. R. Scott, A. Donohoe, and E. R. Newsom (2016), Southern Ocean warming delayed by circumpolar upwelling and equatorward transport, *Nat. Geosci.*, 9(7), 549–554.

Acknowledgments

We thank Brian Rose and an anonymous reviewer for their constructive comments and Yu-Chia Peng and Jia-Ying Tsai for their assistance with figures. Y.-T. Hwang was supported by Ministry of Science and Technology of Taiwan (103-2111-M-002-013, 104-2111-M-002-005, and 105-2628-M-002-009-MY4); S.-P. Xie by the U.S. National Science Foundation (637450); and S. M. Kang by National Research Foundation of Korea (2016R1A1A3A04005520). The NSF-sponsored Climate Simulation Laboratory at NCAR's Computational and Information Systems Laboratory (CISL) provided computing resources on Yellowstone. Request for the idealized experiment outputs can be made to Y.-T. Hwang. The CMIP outputs are available via http://cmip-pcmdi.llnl.gov/cmip5/data_portal.html. We acknowledge the climate modeling groups for producing and making available their model output. The National Center for Atmospheric Research is sponsored by the National Science Foundation.

- Cabre, A., I. Marinov, and A. Ganandesikan (2017), Global atmospheric teleconnections and multi-decadal climate oscillations driven by Southern Ocean convection, *J. Clim.*, doi:10.1175/JCLI-D-16-0741.1.
- Cheng, W., J. C. H. Chiang, and D. Zhang (2013), Atlantic meridional overturning circulation (AMOC) in CMIP5 models: RCP and historical simulations, *J. Clim.*, 26(18), 7187–7197.
- Chiang, J. C. H., and C. M. Bitz (2005), The influence of high latitude ice on the position of the marine Intertropical Convergence Zone, *Clim. Dyn.*, 25, 477–496.
- Chiang, J. C. H., and A. R. Friedman (2012), Extratropical cooling, interhemispheric thermal gradients, and tropical climate change, *Annu. Rev. Earth Planet. Sci.*, 40, 383–412.
- Chiang, J. C. H., Y. Fang, and P. Chang (2008), Interhemispheric thermal gradient and tropical Pacific climate, *Geophys. Res. Lett.*, 35, L14704, doi:10.1029/2008GL034166.
- de Boyer Montégut, C., G. Madec, A. S. Fischer, A. Lazar, and D. Iudicone (2004), Mixed layer depth over the global ocean: An examination of profile data and a profile-based climatology, *J. Geophys. Res.*, 109, C12003, doi:10.1029/2004JC002378.
- Deser, C., M. A. Alexander, S. P. Xie, and A. S. Phillips (2010), Sea surface temperature variability: Patterns and mechanisms, *Annu. Rev. Mar. Sci.*, 2, 115–143.
- Deser, C., R. A. Tomas, and L. Sun (2015), The role of ocean–atmosphere coupling in the zonal-mean atmospheric response to Arctic sea ice loss, *J. Clim.*, 28(6), 2168–2186.
- Donohoe, A., J. Marshall, D. Ferreira, K. Armour, and D. McGee (2014), The interannual variability of tropical precipitation and interhemispheric energy transport, *J. Clim.*, 27(9), 3377–3392.
- Fedorov, A. V., N. J. Burls, K. T. Lawrence, and L. C. Peterson (2015), Tightly linked zonal and meridional sea surface temperature gradients over the past five million years, *Nat. Geosci.*, 8(12), 975.
- Friedman, A. R., Y.-T. Hwang, J. C. H. Chiang, and D. M. W. Frierson (2013), Interhemispheric temperature asymmetry over the twentieth century and in future projections, *J. Clim.*, 26, 5419–5433.
- Frierson, D. M., and Y. T. Hwang (2012), Extratropical influence on ITCZ shifts in slab ocean simulations of global warming, *J. Clim.*, 25(2), 720–733.
- Frölicher, T. L., J. L. Sarmiento, D. J. Paynter, J. P. Dunne, J. P. Krasting, and M. Winton (2015), Dominance of the Southern Ocean in anthropogenic carbon and heat uptake in CMIP5 models, *J. Clim.*, 28, 862–886.
- Green, B., and J. Marshall (2017), Coupling of trade winds with ocean circulation damps ITCZ shifts, *J. Clim.*, 30(12), 4395–4411.
- Hawcroft, M., J. M. Haywood, M. Collins, A. Jones, A. C. Jones, and G. Stephens (2016), Southern Ocean albedo, inter-hemispheric energy transports and the double ITCZ: Global impacts of biases in a coupled model, *Clim. Dyn.*, 1–17.
- He, J., C. Deser, and B. J. Soden (2017), Atmospheric and Oceanic Origins of Tropical Precipitation Variability, *J. Clim.*, 30(9), 3197–3217.
- Held, I. M. (2001), The partitioning of the poleward energy transport between the tropical ocean and atmosphere, *J. Atmos. Sci.*, 58(8), 943–948.
- Held, I. M., M. Winton, K. Takahashi, T. Delworth, F. Zeng, and G. K. Vallis (2010), Probing the fast and slow components of global warming by returning abruptly to preindustrial forcing, *J. Clim.*, 23(9), 2418–2427.
- Hill, S. A., Y. Ming, and I. M. Held (2015), Mechanisms of forced tropical meridional energy flux change, *J. Clim.*, 28, 1725–1742.
- Hwang, Y. T., and D. M. Frierson (2013), Link between the double-Intertropical Convergence Zone problem and cloud biases over the Southern Ocean, *Proc. Natl. Acad. Sci.*, 110(13), 4935–4940.
- Hwang, Y.-T., D. M. W. Frierson, and S. M. Kang (2013), Anthropogenic sulfate aerosol and the southward shift of tropical precipitation in the late 20th century, *Geophys. Res. Lett.*, 40, L50502, doi:10.1002/grl.50502.
- Intergovernmental 428 Panel on Climate Change (2014), *Climate Change 2014: Synthesis Report. Contribution of Working Groups I, II and III to the Fifth Assessment Report of the Intergovernmental Panel on Climate Change*, edited by Core writing team, R. K. Pachauri, and L. A. Meyer, 151 pp., IPCC, Geneva, Switzerland.
- Jia, F., and L. Wu (2013), A study of response of the equatorial Pacific SST to doubled-CO₂ forcing in the coupled CAM-1.5-layer reduced-gravity ocean model, *J. Phys. Oceanogr.*, 43(7), 1288–1300.
- Kang, S. M., I. M. Held, D. M. W. Frierson, and M. Zhao (2008), The response of the ITCZ to extratropical thermal forcing: Idealized slab-ocean experiments with a GCM, *J. Clim.*, 21(14), 3521–3532.
- Kay, J. E., C. Wall, V. Yettella, B. Medeiros, C. Hannay, P. Caldwell, and C. Bitz (2016), Global climate impacts of fixing the Southern Ocean shortwave radiation bias in the Community Earth System Model (CESM), *J. Clim.*, 29(12), 4617–4636.
- Kuhlbrodt, T., and J. M. Gregory (2012), Ocean heat uptake and its consequences for the magnitude of sea level rise and climate change, *Geophys. Res. Lett.*, 39, L18608, doi:10.1029/2012GL052952.
- Liu, Z., S. Vavrus, F. He, N. Wen, and Y. Zhong (2005), Rethinking tropical ocean response to global warming: The enhanced equatorial warming, *J. Clim.*, 18(22), 4684–4700.
- Manabe, S., R. J. Stouffer, M. J. Spelman, and K. Bryan (1991), Transient responses of a coupled ocean-atmosphere model to gradual changes of atmospheric CO₂. Part I. Annual mean response, *J. Clim.*, 4(8), 785–818.
- Marshall, J., Armour, K. C., Scott, J. R. Kostov, Y., Hausmann, U., Ferreira, D., Shepherd, T. G., Bitz, C. M. (2014), The ocean's role in polar climate change: Asymmetric Arctic and Antarctic responses to greenhouse gas and ozone forcing, *Phil. Trans. R. Soc. A*, 372(2019), 20130040.
- Raper, S. C., J. M. Gregory, and R. J. Stouffer (2002), The role of climate sensitivity and ocean heat uptake on AOGCM transient temperature response, *J. Clim.*, 15(1), 124–130.
- Roemmich, D., J. Church, J. Gilson, D. Monselesan, P. Sutton, and S. Wijffels (2015), Unabated planetary warming and its ocean structure since 2006, *Nat. Clim. Change*, 5, 240–254.
- Rose, B. E., and M. C. Rencurrel (2016), The vertical structure of tropospheric water vapor: Comparing radiative and ocean-driven climate changes, *J. Clim.*, 29(11), 4251–4268.
- Rose, B. E. J., K. C. Armour, D. S. Battisti, N. Feldl, and D. B. Koll (2014), The dependence of transient climate sensitivity and radiative feedbacks on the spatial pattern of ocean heat uptake, *Geophys. Res. Lett.*, 41, 1071–1078, doi:10.1002/2013GL058955.
- Rugenstein, M. A., K. Caldeira, and R. Knutti (2016), Dependence of global radiative feedbacks on evolving patterns of surface heat fluxes, *Geophys. Res. Lett.*, 43, 9877–9885, doi:10.1002/2016GL070907.
- Schneider, T., T. Bischoff, and G. H. Haug (2014), Migrations and dynamics of the intertropical convergence zone, *Nature*, 513, 45–53.
- Ting, M., and P. D. Sardeshmukh (1993), Factors determining the extratropical response to equatorial diabatic heating anomalies, *J. Atmos. Sci.*, 50(6), 907–918.
- Tomas, R. A., C. Deser, and L. Sun (2016), The role of ocean heat transport in the global climate response to projected Arctic sea ice loss, *J. Clim.*, 29(19), 6841–6859.

- Trenberth, K. E., G. W. Branstator, D. Karoly, A. Kumar, N. C. Lau, and C. Ropelewski (1998), Progress during TOGA in understanding and modeling global teleconnections associated with tropical sea surface temperatures, *J. Geophys. Res.*, *103*, 14,291–14,324, doi:10.1029/97JC01444.
- Xie, S. P., C. Deser, G. A. Vecchi, J. Ma, H. Teng, and A. T. Wittenberg (2010), Global warming pattern formation: Sea surface temperature and rainfall, *J. Clim.*, *23*, 966–986.
- Xie, S.-P., B. Lu, and B. Xiang (2013), Similar spatial patterns of climate responses to aerosol and greenhouse gas changes, *Nat. Geosci.*, *6*, 828–832.
- Wang, C., L. Zhang, S. K. Lee, L. Wu, and C. R. Mechoso (2014), A global perspective on CMIP5 climate model biases, *Nat. Clim. Change*, *4*(3), 201–205.
- Zhang, R., and T. L. Delworth (2005), Simulated tropical response to a substantial weakening of the Atlantic thermohaline circulation, *J. Clim.*, *18*(12), 1853–1860.
- Zhang, L., and T. Li (2014), A simple analytical model for understanding the formation of sea surface temperature patterns under global warming, *J. Clim.*, *27*(22), 8413–8421.